New Relationships for Two-Phase Turbulent Mixing and Buoyancy Drift in Rod Bundles

L.N. Carlucci, N. Hammouda and D.S. Rowe[*]

Atomic Energy of Canada Limited
Chalk River Laboratories
Chalk River, Ontario, Canada, K0J 1J0
[*]*Rowe and Associates, Woodinville, WA, USA*

1. INTRODUCTION

Subchannel-based computer codes are routinely used to assess the thermalhydraulic behaviour of fuel assemblies in nuclear reactors [1-3]. Such assessments are important, particularly in determining the CHF (Critical Heat Flux), which limits the maximum thermal power that can be extracted from the fuel for a given set of thermalhydraulic operating conditions. These codes solve the 1D (one-dimensional) conservation equations of mass momentum and energy for each interconnected subchannel. Interactions leading to the intersubchannel exchange of mass, energy and momentum are modelled as semi-empirical source terms to the 1D equations. The key mechanisms associated with these interactions are generally accepted to be as follows [4-6]:

1) *Single- and two-phase diversion cross-flow*. Directed flow caused by a net transverse pressure difference between adjacent subchannels. Lateral pressure differences can result from different subchannel hydraulic diameters, heat flux distributions and gradual and abrupt changes in flow areas caused, for example, by element bowing and spacer grids, respectively.

2) *Single- and two-phase turbulent mixing*. This is a result of random turbulent flow and pressure fluctuations. It can be further classified as natural or forced. Natural turbulent mixing occurs continuously between smooth interconnected subchannels. Forced turbulent mixing results from the non-directional flow scattering caused by local flow obstructions such as bundle junctions, spacers, bearing pads, and grids. Mixing caused by non-directional flow scattering is in addition to any directed, diversion cross-flow caused by the obstruction if it is non-symmetric (i.e., more obstruction in one subchannel than in the other). Under single-phase flow conditions, density differences between interconnected subchannels at different temperatures are negligible and thus there is a net transfer of thermal energy from the higher- to the lower-temperature subchannel, but negligible mass transfer. Under two-phase conditions, the turbulent fluctuations of the liquid and gas phases can result in a net mass transfer, in addition to a net energy transfer between two interconnected subchannels having different void fractions.

3) *Two-phase void drift*. This is due to the tendency of the vapour phase to redistribute itself to a preferred “equilibrium” void distribution [5]. In a bundle comprising subchannels of different sizes and shapes the "equilibrium" void fraction in the larger subchannels tends to be higher than in the smaller ones. This has been observed in both low-pressure, adiabatic air-water conditions [7] and high-pressure, diabatic steam-water conditions [8,9].

4) *Two-phase gravity-induced buoyancy drift in horizontal channels*. This results from the tendency of the lighter gas phase to move upwards with respect to the heavier liquid phase. The net effect is an increase in void fraction with height in the lateral direction. It can be important at the lower mass fluxes encountered in off-normal CANDU reactor conditions.

All of the above mechanisms affect the lateral distributions of phasic energy (enthalpy) in both single- and two-phase flow, and phasic density or void fraction in two-phase flow. These in turn affect the CHF location and magnitude, the axial pressure drop, the extent of void generation before CHF, and post-dryout (PDO) heat transfer. It is thus important to understand these mechanisms and to accurately quantify their behaviour.

Following a review of available data and models for single- and two-phase turbulent mixing, new relationships were developed to treat intersubchannel turbulent mixing in a unified way under both single- and two-phase flow conditions. These models, together with an available relation for void drift, were implemented in the ASSERT-PV subchannel thermalhydraulics code [1], and assessed using a range of data on enthalpy migration in vertical flow under BWR and PWR conditions. The intent of this assessment was to optimize these relationships to give the best agreement with the enthalpy migration data for vertical flows. The optimized turbulent mixing relationships were then used to improve the treatment of buoyancy drift in horizontal flows typical of CANDU reactor normal and off-normal conditions.

This paper presents the new relationships, together with selected results of the optimization and assessment.

2. TURBULENT MIXING AND VOID DRIFT

2.1 Single-Phase Turbulent Mixing

A recent, comprehensive state-of-the-art review carried out by Rehme [10] indicates that the mechanisms governing intersubchannel turbulent mixing in single-phase flow are generally well understood. Numerous correlations and models developed over the last 40 years indicate that single-phase turbulent mixing is a function of axial Reynolds number, Re, and geometry, with the latter characterized by the gap-to-diameter ratio, *S/d*, and tube arrangement, which determines subchannel type (i.e., triangular-triangular subchannels, square-square, and triangular-square). The various relationships for the single-phase turbulent mixing rate per unit length, w', can be recast in terms of a mixing factor, *Y*, which can be interpreted as the ratio of gap diffusivity, *e*, to a reference diffusivity, e_r, normally taken as that at the centre of a circular pipe [10,11]

$$Y = \left(\frac{w'}{\rho e_r} \right) \left(\frac{\Delta y}{S} \right) = \frac{e}{e_r}; \qquad e = \left(\frac{w'}{\rho} \right) \left(\frac{\Delta y}{S} \right) \tag{2.1}$$

where *Dy* and ρ are the centroidal distance and fluid density respectively. The magnitude of the mixing factor is significantly greater than one, indicating that mixing in the gap is greater than that in the centre of a pipe for the same Reynolds number, and tends to increase with decreasing gap-to-diameter ratio [10]. There is a consensus that the high mixing rate in the gap is due to macroscopic pulsations of flow in the gap, and not to secondary flows in the vicinity of the gap, as previously thought [10]. Despite the good understanding of the governing mechanisms, the available relationships tend to give a wide range of mixing rates for the same nominal Reynolds number and geometry. This is attributed to differences in geometric tolerances of the test sections, differences in measurement techniques, disturbances of the flow field by grid spacers (where used) and probes, and by inadequate development lengths [10]. The presence of upstream obstructions such as grid spacers will generally result in higher mixing rates than obtained with smooth subchannels, with the magnitude of the increase dependent on the degree of flow area blockage by the obstruction.

2.2 Two-Phase Turbulent Mixing

In general, both the level of understanding and the supporting data on two-phase mixing are significantly less than for single-phase flow [12]. Virtually all mixing experiments have been conducted under adiabatic conditions in air-water at low pressures (0.1-0.34 MPa) over the mass-flux range of 100-2000 kg/m²/s [13-17]. The diabatic, steam-water experiments of Rowe and Angle [18] are the only ones that provide mixing data at more realistic pressure (2.8 and 5.2 MPa) and mass flux (1060-4070 kg/m²/s) conditions. However, these still fall short of CANDU reactor normal operating conditions, which are nominally at 10 MPa with mass fluxes up to 7000 kg/m²/s. Nonetheless, although there is a great deal of scatter in the measured mixing rates, results from these experiments provide a number of useful observations, which can be used as a basis to develop improved models and correlations compared to those that are currently available. The following are some of the important points:

- Two-phase mixing is a strong function of flow regime (Figure 1). The liquid mixing rate starts at the single-phase value, reaches a maximum in the slug/churn regime and monotonically decreases beyond the slug/churn-annular transition. The gas mixing rate starts near-zero values at low qualities, reaches a maximum near the slug/churn-annular transition and decreases to the single-phase gas value as 100% quality is approached. Maximum phasic mixing rates are about one order of magnitude greater than their corresponding single-phase values.
- When normalized by their respective axial flow-rates, phasic mixing rates decrease with increasing mass flux, with the extent of the decrease being a function of both mass flux and system pressure.
- Phasic mixing rates are relatively insensitive to gap spacing at values above ~ 1.5 mm, but tend to decrease with decreasing gap spacing at levels below this value.
- Array geometry (i.e., triangular or square arrangements) does not appear to affect two-phase mixing in a systematic way.
- Low-pressure air-water experiments have shown that the mixing rate of the liquid correlates well with the RMS value of the instantaneous pressure difference between interconnected subchannels [17]. This, together with visual observations of the movement and interaction of liquid slugs between the interconnected subchannels, suggests that the increased level of mixing in two-phase flow compared to single-phase flow is caused by fluctuating transverse pressure differences that result from the non-synchronous movement of liquid and gas slugs in the interconnected subchannels.

On the basis of the above observations, and additional considerations on the effects of flow obstructions when present, the following new relationships for $w_l^{'}$ and $w_g^{'}$, the liquid and gas-phase mixing rates per unit length were developed:

$$w_l^{'} = w_{l,\mathrm{hom}}^{'} + w_{l,inc}^{'}; \qquad w_{l,\mathrm{hom}}^{'} = F_{obs}(1-x)w_{\mathrm{hom}}^{'} \text{ and } w_{l,inc}^{'} = \frac{F_{G,P}F_{gap}\Delta w_{l,2j}^{'}}{F_{obs}} \tag{2.2}$$

$$w_g^{'} = w_{g,\mathrm{hom}}^{'} + w_{g,inc}^{'}; \qquad w_{g,\mathrm{hom}}^{'} = F_{obs}xw_{\mathrm{hom}}^{'} \text{ and } w_{g,inc}^{'} = \frac{F_{G,P}F_{gap}\Delta w_{g,2j}^{'}}{F_{obs}} \tag{2.3}$$

The correlation forms defined by Equations (2.2) and (2.3) were chosen on the assumption that when the two-phase flow is homogeneous, the total gas and liquid mixing rate can be adequately estimated from the single-phase flow relationship based on the use of the homogeneous viscosity. Hence, the parameters $\Delta w_{l,2j}^{'}$ and $\Delta w_{g,2j}^{'}$ can be interpreted as the additional (or incremental) two-phase mixing components of the liquid and gas phases above the corresponding homogeneous flow values, resulting from flow-regime

enhancement effects due to the inhomogeneous nature of the flow (e.g., the movement of non-synchronous slugs in pairs of interconnected subchannels).

The obstruction factor F_{obs}, is introduced to account for additional mixing above the homogeneous value caused by flow obstructions such as spacer grids and end plates. It is assumed to increase the homogeneous component of mixing and to decrease the incremental component, since obstructions are expected to homogenize the flow downstream. Since two-phase flow data is lacking, it is based on the observations of heat transfer and the decay of turbulence downstream of obstructions under single-phase flow conditions [19,20]. The following relation was developed for this study:

$$F_{obs} = 1 + a_{obs} k \exp\left(- b_{obs} \frac{z}{d_h} \right) \tag{2.4}$$

where k and z are the obstruction loss coefficient and downstream distance from the obstruction, respectively, d_h is the hydraulic diameter, and the recommended values of the constants a_{obs} and b_{obs} are 3.3 and 0.13.

The gap factor, F_{gap}, is introduced to account for the reduction in two-phase mixing rates with decreasing gap. It is given by:

$$F_{gap} = 1.287\left[1 - \exp\left(-1.5 \cdot 10^6 S^2\right)\right] \tag{2.5}$$

The mass flux and pressure-dependent factor $F_{G,P}$ is based on simplified criteria for the transition from slug/churn to the dispersed bubbly flow regime [21], and is designed to account for the decrease in mixing rates at higher mass fluxes and pressures [18]. The following form was developed for this study:

$$F_{G,P} = \exp\left[- a_{G,P} \left(b_{G,P} - \min\left(b_{G,P}, R_{G,P}\right)\right)^2\right] \tag{2.6}$$

where:

$$R_{G,P} = \frac{d_C}{\min\left(d_{CD}^{Br}, d_{CB}\right)} \tag{2.7}$$

In the above, d_C is maximum stable bubble size necessary to maintain dispersed bubbly flow, d_{CD}^{Br} is the Brodkey [22] expression for the critical bubble size above which the bubble is deformed, and d_{CB} is the critical bubble size above which migration of bubbles to the upper part of a horizontal or inclined pipe occurs. In general, there will be a tendency to remain in the dispersed bubbly flow regime as long as turbulence levels are high enough to keep d_C less than either d_{CD}^{Br} or d_{CB}. The variation of $F_{G,P}$ with mass flux and system pressure is illustrated in Figure 2, using recommended values of 11.0 and 0.9 for $a_{G,P}$ and $b_{G,P}$, respectively.

The Rogers and Tahir relations [23] are used to define w'_{hom}, the homogeneous flow mixing rate per unit length:

$$\frac{w'_{\text{hom}}}{m_{\text{hom}}} = a_w \left(\frac{S}{d}\right)^{b_w} \left(\frac{Gd_h}{m_{\text{hom}}}\right)^{0.9}_{\text{hom}}; \quad m_{\text{hom}} = \left(\frac{x}{m_g} + \frac{1-x}{m_l}\right)^{-1} \tag{2.8}$$

where G, d, x and m are the mass flux, fuel element diameter, flow quality and dynamic viscosity, respectively, and the constants a_w and b_w are equal to 0.0018 and -0.4 for triangular arrays, and to 0.005 and 0.106 for square arrays. The incremental phasic mixing rates are a fit to the low-pressure air-water data of Rudzinski and co-workers[1] [13-15]:

$$\Delta w'_{l,2j} = 0.0515 \exp\left[-0.5\left(\frac{a-0.53}{0.1794}\right)^2\right] \tag{2.9}$$

$$\Delta w'_{g,2j} = 0.00264 \exp\left[-8.332\{\ln(1-1.9412(a-0.75884))\}^2\right] \tag{2.10}$$

The void fraction, a, was chosen instead of quality, to allow easier application of the correlations to higher pressures. The Chisholm correlation was used to calculate the void fractions from the flow qualities [24]. The level of agreement with the experimental data is illustrated in Figures 3 and 4, which clearly show that the liquid-phase mixing rate peaks at a void fraction of just over 50%, whereas the gas mixing rate peaks at a void fraction of just under 80%. Figure 5 shows that the new relationships, which are based on air-water, together with the factors F_{gap} and $F_{G,P}$, are in good agreement with selected mixing data for diabatic steam-water conditions at higher pressures [18].

The phasic diffusion coefficients are calculated from the corresponding mixing rates using the following:

$$e_g = \left(\frac{w'_g}{r_g a}\right)\left(\frac{\Delta y}{S}\right) \tag{2.11}$$

$$e_l = \left(\frac{w'_l}{r_l (1-a)}\right)\left(\frac{\Delta y}{S}\right) \tag{2.12}$$

Figure 6 shows that the phasic diffusion coefficients differ both in magnitude and functional dependence. In general, the gas-phase diffusion coefficients are significantly higher than the liquid values at void fraction greater than 40%.

---

[1] This was done by first determining the experimental values of the incremental phasic mixing rates from the total values by subtracting the corresponding homogeneous components (using equation (2.8)), and then fitting the resulting data with the incremental mixing relationships (equations (2.9) and (2.10))

2.3 Void Drift

Void drift was modelled with the form used by Rowe et al. [2] to calculate the equilibrium void, $a_{eq,i}$, in a given subchannel as a function of the corresponding hydraulic diameter, $d_{h,i}$, and the cross-sectional averages of the void fraction, $\overline{\overline{a}}$, and hydraulic diameter, $\overline{\overline{d}}_h$:

$$a_{eq,i} = \overline{\overline{a}} + a_{eq} F_{G,P} \overline{\overline{a}} \left(1 - \overline{\overline{a}}\right) \left(1 - \frac{\overline{\overline{d_h}}}{d_{h,i}}\right) \tag{2.13}$$

The coefficient a_{eq} was determined in this study to be 0.85, from a re-examination of the air-water experiments of Sterner and Lahey [7]. Note that the factor $F_{G,P}$ is used since a non-uniform equilibrium void distribution corresponding to different subchannel sizes is assumed to disappear at high enough mass fluxes and system pressure when the two-phase flow structure is expected to become homogeneous.

3. BUOYANCY DRIFT

A Wallis-type relationship for the buoyancy drift velocity was developed and assessed. The new relationship was developed to account for two effects that are important when considering the buoyancy-induced motion of the gas phase relative to the liquid phase in the lateral direction: the expected reduction of the magnitude of the bubble rise velocity as the mean bubble size approaches the width of the gap, and the expected reduction of the surface roughness of the liquid film in annular flow for a given mass flux as the system pressure is increased, resulting largely from a decrease in the gas-phase velocity. The reduction in the surface roughness is postulated to result in less obstruction of the narrow gap by the liquid film and hence in an increase in the relative gas velocity in the lateral direction.

The form of the proposed relationship for V_{gj}, the buoyancy-drift velocity, is as follows:

$$V_{gj} = F_{G,P} V_{gj0} \left[1 + (\Lambda - 1)\Xi\right] a_P \left(1 - a\right)^{b_P} \tag{3.1}$$

where the rise velocity of a single bubble in a stagnant liquid phase, V_{gj0} is given by:

$$V_{gj0} = a_{gj} \left[\frac{\left(r_l - r_g\right) s g}{r_l^2}\right]^{0.25} \tag{3.2}$$

and:

$$\Lambda = \begin{cases} 1 - \dfrac{d_{CD}^{Br}}{0.9S} & for\ \dfrac{d_{CD}^{Br}}{S} < 0.6 \\ 0.12 \left(\dfrac{d_{CD}^{Br}}{S}\right)^{-2}; & for\ \dfrac{d_{CD}^{Br}}{S} \geq 0.6 \end{cases} \tag{3.3}$$

The above expressions for Λ are those proposed by Wallis [25] to account for the reduction of the bubble rise velocity in a small-diameter vertical tube, with the vessel diameter replaced by the gap width. Since

this effect is expected to dominate in the bubbly flow regime, the additional factor Ξ was introduced to ensure that the correction factor approaches a magnitude of one at the end of the bubbly flow regime. The additional factor is defined by:

$$\Xi = \exp\left\{-\left[\left(\frac{a}{a_{bs}}\right)\left(\frac{S}{d_{CD}^{Br}}\right)\right]^{c}\right\} \tag{3.4}$$

where the a_{bs}, the void fraction at the bubble-slug transition, and the exponent, c are selected to give best agreement with data (see Section 5.2). The pressure-dependent coefficient and exponent are defined as follows:

$$a_P = \begin{cases} 1 & ; a < a_{sa} \\ (1 - a_{sa})^{(b_l - b)} & ; a \geq a_{sa} \end{cases} \tag{3.5}$$

$$b_P = \begin{cases} b_l & ; a < a_{\mathrm{sa}} \\ b & ; a \geq a_{\mathrm{sa}} \end{cases} \tag{3.6}$$

$$\begin{aligned} b &= b_l + 0.2(b_h - b_l)(P_{term} - 5.0) \\ P_{term} &= \max\left[5.0, \min\left(10.0, P_{ref}\right)\right] \end{aligned} \tag{3.7}$$

In the above, s is the surface tension, a_{sa} is the void fraction at the slug-annular transition and P_{ref} is the reference system pressure.

4. IMPLEMENTATION

The above relationships for turbulent mixing and void drift were implemented in the ASSERT-PV code [1], which is based on the drift flux model of two-phase flow. Two methods of implementation were investigated: fully explicit and semi-implicit. In the fully explicit method, separate phasic diffusion coefficients were used to calculate the intersubchannel turbulent fluxes of mass, energy and momentum. These turbulent flux terms were included as explicit source terms in each governing equation. In the semi-implicit method, only the components of the energy and momentum turbulent fluxes due to intersubchannel enthalpy and axial velocity gradients were based on separate phasic diffusion coefficients, and incorporated as explicit source terms in the corresponding conservation equation. The components of mass, energy and momentum transfer due to intersubchannel void gradients were based on a single "void" diffusion coefficient calculated from the total, liquid-plus-gas mixing rates. These were then incorporated into each conservation equation implicitly in the form of a lateral void diffusion velocity component of the relative velocity, V_r, which also includes the buoyancy drift component:

$$V_r = V_g - V_l = \frac{V_{gj} + V_{diff}}{1 - a} \tag{4.1}$$

where V_{diff} is the "void" diffusion velocity given by:

$$V_{diff} = -\left(\frac{e}{a}\right)\frac{\Delta\left(a - a_{eq}\right)}{\Delta y} \tag{4.2}$$

with the void diffusion coefficient defined by:

$$e = e_{\hom} + e_{inc} \Rightarrow e_{\hom} = \left(\frac{w'_{g,\hom} + w'_{l,\hom}}{r}\right)\left(\frac{\Delta y}{S}\right) \text{ and } e_{inc} = \Omega\left(\frac{w'_{g,inc} + w'_{l,inc}}{r}\right)\left(\frac{\Delta y}{S}\right) \tag{4.3}$$

The incremental mixing factor Ω, is introduced in anticipation of the optimization that follows when assessing the enthalpy migration data. The two methods yield virtually identical results. Hence, since the semi-implicit method is more robust, and is more easily accommodated into the ASSERT-PV framework, it was retained.

5. ASSESSMENT

Overall, ten data sets were assessed, eight on enthalpy migration in the outlet of selected subchannels in vertical flow [8,9,26-28], and two data sets on air-water void migration [29], and steam-water enthalpy migration in horizontal flow [30]. Table 1 lists key data on geometry and operating conditions.

5.1 Vertical Flow

The GE (General Electric) data on the uniformly heated 9-rod bundle, with low resistance grid spacers [9], was used to optimize the new mixing relationships via the incremental mixing factor, Ω. Figure 7 indicates that a value of three for the incremental mixing factor results in the lowest mean errors of qualities and mass fluxes in the corner subchannel, and the corner, side and centre subchannels combined. RMS errors show similar trends. Consequently, this value was used in all subsequent assessments.

A value of one, which indicates the use of the original relationships without any modification, clearly results in mean and RMS errors that are too high. This implies that the mixing rates required to yield the right levels of enthalpy migration due to combined void diffusion and void drift, are significantly higher then obtained from relationships based on data from liquid-to-liquid and gas-to-gas mass transfer experiments done with passive tracers. However, the good agreement obtained using a constant value of the incremental mixing factor, indicates that the degree of additional or incremental mixing above the value obtained assuming homogeneous flow, is a reasonable way to quantify the degree of void diffusion and void drift, when used in conjunction with the equilibrium void concept as characterized by the Rowe et al. model [2].

Table 2 summarizes mean and RMS errors between calculated and predicted qualities and mass fluxes for the various data sets. Selected comparisons between predicted and measured subchannel outlet qualities are illustrated in Figures 8 to 10. Overall, the performance of the new relationships is considered good, particularly in the prediction of qualities. Agreement with data using the new results is significantly better than obtained with an existing model for void diffusion [29] currently used in ASSERT-PV.

5.2 Horizontal Flow

Values of 2.2, 1.5, 0.35 and 4 for the parameters a_{gj}, b_P a_{bs}, and c (in Equations (3.1), (3.2) and (3.4)) were used and confirmed to be appropriate by examining predictions of selected École Polytechnique air-water data on axial void distribution at two mean outlet void fractions, a high value of ~55%, and a low value of ~20%. Figure 11 indicates that with these values, the gap-effect correction results in a reduction of the lateral bubble rise velocity only for the case with the low mean void fraction, thereby confirming the experimental trends. In general, good agreement between predicted and measured void fractions were obtained for the other operating conditions and configurations.

The use of a constant coefficient and exponent in the modified Wallis-type model (a_{gj} = 2.2, a_p = 1, b_p =b_l= 1.5)), with only gap effects accounted for (a_{bs} = *0.35*, c = 4), generally gives good agreement with measured data at qualities of up to about 40%. Above 40% quality, and especially at higher pressures, the buoyancy drift effects are underestimated (i.e., predicted enthalpy migration from the lower to the upper subchannel is lower than measured). Figure 12 shows excellent agreement between predicted and measured outlet qualities using a pressure-dependent coefficient and exponent based on the following values for the constants in the buoyancy drift relation: a_{gj} = 2.2, a_{bs} = *0.35*, c = 4, a_{sa} = 0.7, b_l = 1.5 and b_h = 0.6.

6. CONCLUSIONS

Generalized relationships for intersubchannel turbulent mixing and lateral buoyancy drift in horizontal channels have been developed to handle a wide range of conditions, including those typical of CANDU reactor normal operation.

The relationships for turbulent mixing, together with a recommended one for void drift, have been implemented in a version of the ASSERT-PV subchannel thermalhydraulics code, and assessed using a range of data on enthalpy migration in vertical steam-water flows under BWR and PWR diabatic conditions. The intent of this assessment was to optimize these relationships to give the best agreement with the enthalpy migration data for vertical flows. The optimized turbulent mixing relationships were then used as a basis to benchmark a proposed buoyancy drift model to give the best predictions of void and enthalpy migration data in horizontal flows typical of CANDU reactor operation under normal and off-normal conditions.

Overall, the optimized mixing and buoyancy drift relationships have been found to predict the available data quite well, and considerably better than currently used models. This is expected to result in more accurate calculations of subchannel distributions of phasic flows, and hence, in improved CHF predictions.

REFERENCES

1. M.B. Carver, J.C. Kiteley, R.Q.-N. Zhou, S.V. Junop, D.S. Rowe, *"Validation of the ASSERT Subchannel Code: Prediction of Critical Heat Flux in Standard and Nonstandard CANDU Bundle Geometries,"* Nuclear Technology, Vol. 112, 1995 December.
2. D.S. Rowe, R.B. Macduff, R.E. Collingham, *"Thermalhydraulic Subchannel Model Based on Void Drift,"* Paper No. 9-TPF-02, 9th Int. Heat Transfer Conf., Jerusalem, Israel, 1990.
3. L. Wolf, K. Fischer, H. Herkenrath, W. Hufschmidt, *"Comprehensive Assessment of the ISPRA BWR and PWR Subchannel Experiments and Code Analysis with Different Two-Phase Models and Solution Schemes,"* Nuclear Eng. and Design, Vol. 99, pp. 329-350, 1987.
4. J.T. Rogers, N.E. Todreas, *"Coolant Interchannel Mixing in Reactor Fuel Rod Bundles - Single Phase Coolants,"* Paper in Heat Transfer in Rod Bundles, ASME, 1968 December.

5. R.T. Lahey, Jr., F.J. Moody, The Thermalhydraulics of a Boiling Water Nuclear Reactor, Chapter 4, American Nuclear Society, 1993 (Second Edition).
6. P. Tye, A. Teyssedou, A. Tapucu, *"An Investigation of the Constitutive Relations for Intersubchannel Transfer Mechanisms in Horizontal Flows as Applied in the ASSERT-4 Subchannel Code,"* Nuclear Eng. and Design, Vol. 149, pp. 207-220, 1994.
7. R.W. Sterner, R.T. Lahey Jr., *"Air-Water Subchannel Measurements of the Equilibrium Quality and Mass Flux Distribution in a Rod Bundle,"* U.S. Nuclear Regulatory Commission Report, REP/NUREG-CR-3373/1983, 1983 July.
8. R.T. Lahey, Jr., B.S. Shirilkar, D.W. Radcliffe, *"Two-Phase Flow and Heat Transfer in Multi-Rod Geometries: Subchannel and Pressure Drop Measurements in a Nine-Rod Bundle for Diabatic and Adiabatic Conditions,"* General Electric AEC Research and Development Report, GEAP-13049, 1970 March.
9. H. Herkenrath, W. Hufschmidt, U. Jung , F. Weckermann, *"Experimental Investigation of the Enthalpy and Mass Flow - Distribution in 16-Rod Clusters with BWR - PWR - Geometries and Conditions,"* Commission of the European Communities, Ispra Joint Research Centre Report, EUR 7575 EN, 1981.
10. K. Rehme, *"The Structure of Turbulence in Rod Bundles and the Implications on Natural Mixing Between Subchannels,"* Int. J. Heat and Mass Transfer, Vol. 35, No. 2, 1992.
11. L. Ingesson, S. Hedberg, *"Heat Transfer Between Subchannels in a Rod Bundle,"* Paper in Heat Transfer 1970, Vol. 3, Elsevier, Amsterdam, 1970.
12. J. Weisman, R. W. Bowring, *"Methods for Detailed Thermalhydraulic Analysis of Water-Cooled Reactors,"* Nuclear Science and Eng., Vol. 57, 1975.
13. K.F. Rudzinski, *"Two-Phase Turbulent Mixing for Air-Water Flows in Adjacent Triangular Subchannels,"* M.A.Sc., Department of Chemical Engineering, University of Windsor, 1970.
14. K.S. Singh, *"Air-Water Turbulent Mixing in Simulated Rod Bundle Geometries,"* Ph.D. Thesis, Department of Chemical Engineering, University of Windsor, 1972.
15. F.B. Walton, *"Turbulent Mixing Measurements for Single-Phase Air, Single-Phase Water, and Two-Phase Air-Water Flows in Adjacent Triangular Subchannels,"* M. A. Sc. Thesis, Department of Chemical Engineering, University of Windsor, 1969.
16. M. Sadatomi, A. Kawahara, Y. Sato, *"Turbulent Mixing of Both Gas and Liquid Phases Between Subchannels in Two-Phase Hydrodynamically Equilibrium Flows,"* Proc. Int. Symp. Two-Phase Flow Modelling and Experimentation, Vol. 1, G.P. Celata and R.K. Shah, Editors, Rome, pp. 403-409, 1995.
17. A. Kawahara, Y. Sato, M. Sadatomi, *"The Turbulent Mixing Rate and the Fluctuations of Static Pressure Difference Between Adjacent Subchannels in a Two-Phase Subchannel Flow,"* Nuclear Eng. and Design, Vol. 175, pp. 97-106, 1997.
18. D.S. Rowe, C.W. Angle, *"Crossflow Mixing Between Parallel Flow Channels During Boiling - Part III Effect of Spacers on Mixing Between Two Channels,"* Battelle Northwest Report No. BNWL-371 PT3, 1969 January.
19. S.C. Yao, L.E. Hochreiter, W.J. Leech, *"Heat-Transfer Augmentation in Rod Bundles Near Spacer Grids,"* Transactions of the ASME, Vol. 104, 1982 January.
20. S.K. Yang, M.K. Chung, *"Turbulent Flow Through Mixed Spacer Grids in Rod Bundles,"* 1995 National Heat Transfer Conference, HTD-Vol. 316, ASME, 1995.
21. D. Barnea, *"A Unified Model for Predicting Flow-Pattern Transitions for the Whole Range of Pipe Inclinations,"* Int. J. Multiphase Flow, Vol. 13, pp. 1-12, 1987.
22. D. Barnea, O. Shosham, Y. Taitel, *"Flow Pattern Transition for Vertical Downward Two Phase Flow,"* Chem. Eng. Science, Vol. 37, No. 5, pp. 741-744, 1982.
23. J.T. Rogers, A.E.E. Tahir, *"Turbulent Interchange Mixing in Rod Bundles and the Role of Secondary Flows,"* ASME 75-HT-31, 1975.

24. D. Chisholm, *"Research Note: Void Fraction During Two-Phase Flow,"* Journal of Mechanical Engineering Science, Vol. 15, No. 3, pp. 235-236, 1973.
25. G.B. Wallis, One-Dimensional Two-Phase Flow, McGraw Hill, 1969.
26. C. F. Fighetti, D. G. Reddy, *"Experimental Determination of Subchannel Mass Flow Rate and Enthalpy in Rod Bundles,"* Tube Bundle Thermal-Hydraulics, pp. 63-73, ASME, 1982 June.
27. B. Gustafson, R. Harju, O. Imset, *"Flow and Enthalpy Distribution in a 9-Rod Bundle,"* SDS-82, AE-RL-1544. European Two-Phase Flow Meeting, Harwell, 1974 May 22.
28. D. S. Rowe and C. W. Angle, *"Cross Flow Mixing Between Parallel Flow Channels During Boiling, Part II: Measurement of Flow Enthalpy in Two Parallel Channels,"* BNWL-371 Part 2, Pacific Northwest Laboratory, Richland, WA., 1967 December.
29. A. Tapucu, A. Teyssedou, P. Tye, N. Troche, *"The Effect of Turbulent Mixing Models on the Prediction of Subchannel Codes,"* Nuclear Eng. and Design, vol. 149, pp. 221-231, 1994.
30. S.T. Yin, R.M. Tain, G. Chukkapalli, S.C. Sutradhar, *"An Experimental Investigation of Enthalpy/Void Migration in an Equally Heated Twin-Subchannel Assembly,"* Ninth Int. Meeting on Nuclear Reactor Thermalhydraulics, San Francisco, 1999 October 3-8.

Table 1: Relevant geometry and operating conditions for data sets.

Data Sets	Geometry					Operating Conditions			
	Rod Diam. (mm)	Pitch (mm)	Heated Length (m)	Flow Area (cm^2)	Gap (mm)	Press. (MPa)	Mass Flux ($kg/m^2/s$)	Heat Flux (MW/m^2)	$x_{avg,out}$ [$a_{avg,out}$] (%)
GE [8] (3x3) uniform radial heat flux	14.5	18.7	1.83	0.50 Cor. 1.18 Side 1.87 Cen.	4.3 int. 3.4 wall	6.9	720 & 1460	0.7 to 2.1	3 to 32
PELCO-S [9] (4x4)	15.0	19.5	3.66	0.53 Cor. 1.24 Side 2.05 Cen.	4.5 int. 3.4 wall	7.0	900 to 2000	0.1 to 0.8	2 to 32
EUROP [9] (4x4)	10.75	14.3	3.66	0.38 Cor. 0.73 Side 1.14 Cen.	3.6 int. 2.9 wall	7.0	1000 & 2000	0.2 to 1.1	-17 to 24
						16.0	2200 to 3300	0.7 to 1.1	-17 to 21
Columbia [26] (4x4)	14.3	18.7	3.66	0.51 Cor. 1.20 Side 1.91 Cen.	4.4 int. 3.5 wall	6.9	680 to 2710	0.4 to 1.1	-16 to 8
Studsvik [27] (3x3)	12.25 & 12.0	16.3	1.5	0.62/0.63 Cor. 0.98/1.00 Side 1.48/1.50 Cen.	4.1/4.2 int. 3.5/3.7 wall	7.0	900 & 2000	1.1 to 1.5	-6 to 14
PNL [28] (2 sch)	14.3	N/A	1.5	0.36 Tr. 1.11 Sq.	2.1	6.2	1360 to 4100	0 to 2.1	-35 to 34
	14.3	N/A	1.5	0.26 Tr. 0.79 Sq.	0.5	6.2	1360 to 4100	0 to 1.6	-22 to 26
AECL-CRL [30] (2 sch)	4.6 Equiv.	N/A	3.0	0.20	1.8	5.0, 7.5 & 10.0	1600 to 6000	0 to 1.3	-35 to 60
EP [29] (2 sch)	17.6 Equiv.	N/A	1.14*	1.16 Sq.	1.7	0.13 to 0.19	3000	0	[~ 10 to 65]

* interconnected length

Table 2: Summary of error statistics for BWR and PWR data sets.

Data Set	Location	n	Quality		Mass flux	
			e_{mean}	e_{RMS}	e_{mean}	e_{RMS}
Studsvik	Overall	76	-0.009	0.020	0.019	0.096
(3x3)	Row1 - H	19	-0.023	0.030	0.148	0.160
	Row2 - H	19	-0.019	0.026	-0.006	0.052
	Row3 - C	19	0.001	0.005	-0.041	0.065
	Row4 - C	19	0.005	0.007	-0.026	0.063
Columbia	Overall	80	-0.009	0.019	0.108	0.167
(4x4)	C-sch	40	0.004	0.007	0.020	0.046
	H-sch	40	-0.022	0.026	0.195	0.232
GE	Overall	39	0.001	0.019	-0.001	0.067
(3x3)	Cor. - sch	13	0.010	0.026	0.002	0.098
	Side - sch	13	0.002	0.015	-0.020	0.043
	Cen. -sch	13	-0.010	0.013	0.014	0.045
PELCO-S	Overall	844	0.006	0.017	0.062	0.168
(4x4)	Cor. - sch	211	0.008	0.024	0.300	0.316
	Side - sch	211	-0.004	0.011	-0.071	0.076
	Int. - sch	211	0.010	0.013	0.007	0.029
	Cen. - sch	211	0.009	0.017	0.007	0.057
Europ -7 MPa	Overall	245	-0.002	0.020	-0.029	0.082
(4x4)	Cor. - sch	49	-0.001	0.008	-0.156	0.164
	Side3 - sch	49	0.016	0.019	0.038	0.046
	Side1 - sch	49	-0.024	0.037	-0.051	0.064
	Int. - sch	49	0.000	0.007	0.017	0.023
	Cen. - sch	49	-0.001	0.012	0.006	0.023
Europ-16 MPa	Overall	1025	-0.009	0.020	-0.014	0.095
(4x4)	Cor. - sch	205	-0.018	0.024	-0.180	0.181
	Side3 - sch	205	-0.008	0.011	-0.043	0.045
	Side1 - sch	205	-0.026	0.030	0.029	0.036
	Int. - sch	205	0.007	0.011	0.042	0.043
	Cen. - sch	205	-0.001	0.014	0.083	0.085
PNL - 0.5 mm	Overall	56	-0.011	0.021	0.060	0.113
(2 sch)	Tr. - sch	28	-0.014	0.028	0.153	0.156
	Sq - sch	28	-0.008	0.011	-0.033	0.035
PNL - 2.1 mm	Overall	75	-0.001	0.017	0.016	0.071
(2 sch)	Tr. - sch	37	0.000	0.022	0.047	0.097
	Sq - sch	38	-0.002	0.010	-0.014	0.028

* $e_i = \begin{cases} (x_c - x_m)_i, \text{for quality} \\ \left(\dfrac{G_c - G_m}{G_m}\right)_i, \text{for mass flux} \end{cases}$ where $e_{mean} = \dfrac{1}{n}\sum_{i=1}^{n} e_i$ and $e_{RMS} = \sqrt{\dfrac{1}{n}\sum_{i=1}^{n} e_i^2}$

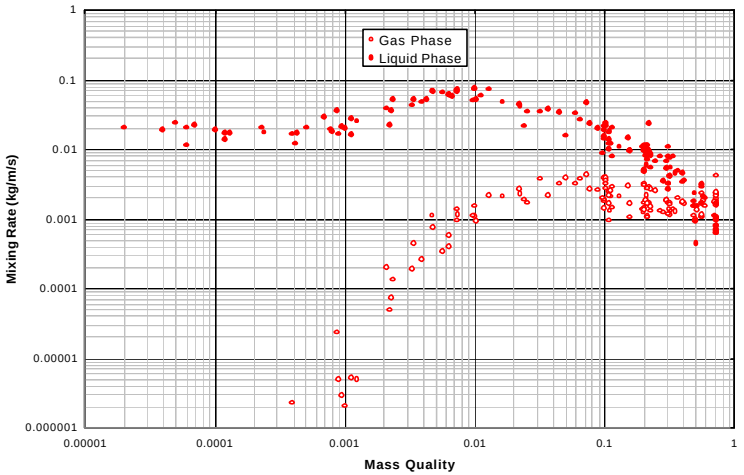

Figure 1: Variation of measured liquid and gas mixing rates with mass quality (air-water data of Rudzinski and co-workers [13-15]).

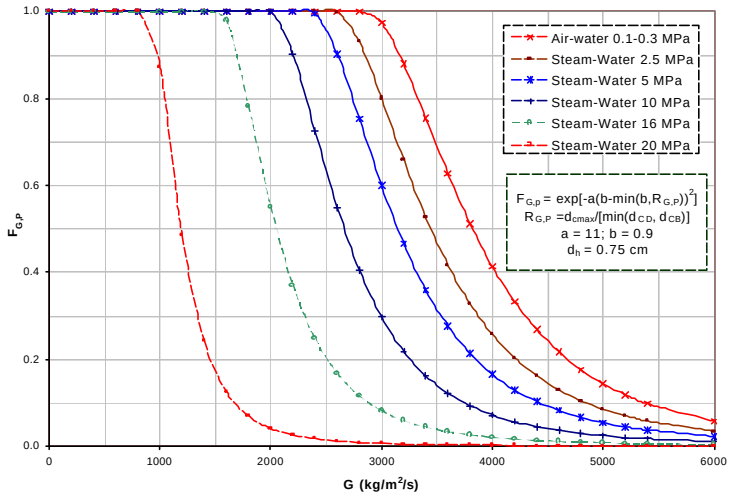

Figure 2: Variation of $F_{G,P}$ with mass flux and pressure.

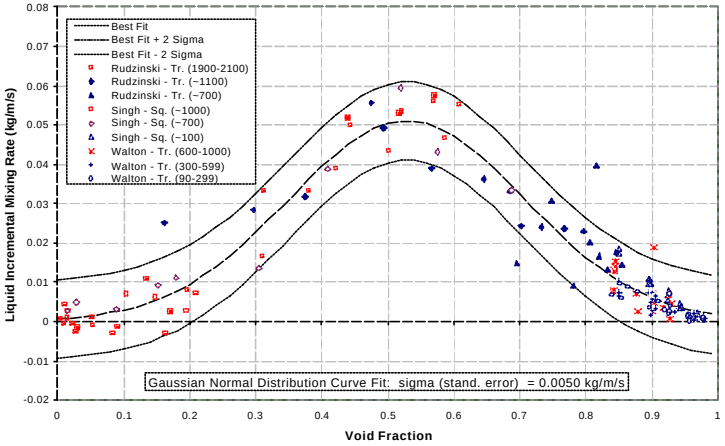

Figure 3: Comparison of predicted and measured incremental two-phase mixing rates for liquid phase.

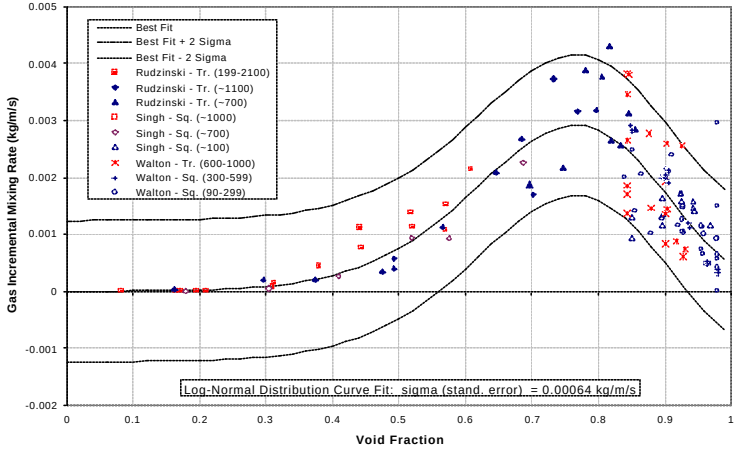

Figure 4: Comparison of predicted and measured incremental two-phase mixing rates for gas phase.

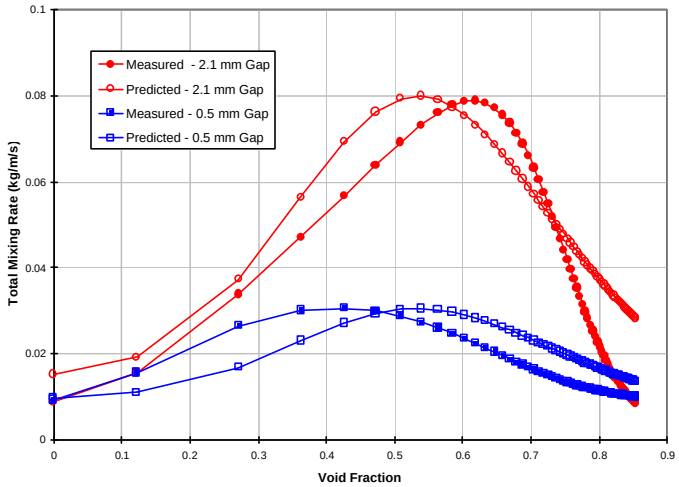

Figure 5: Comparison of Predicted and Measured liquid plus vapour mixing rates for Rowe and Angle 2.1 mm and 0.5 mm gap experiments at 2.8 MPa, 1356 kg/m^2/s.

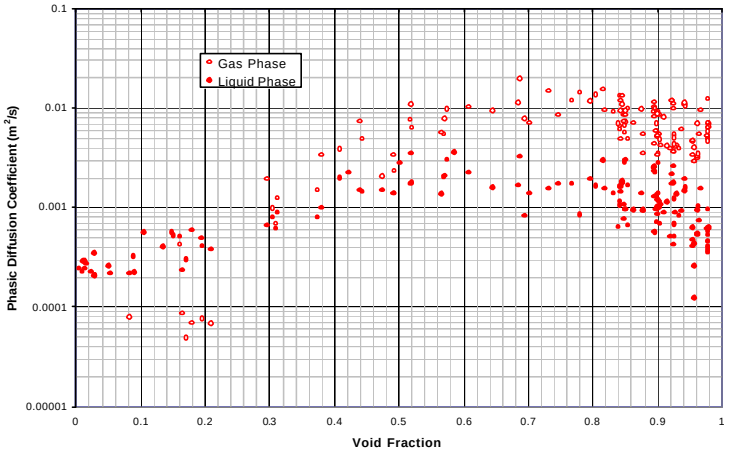

Figure 6: Variation of measured liquid and gas diffusion coefficients with void fraction (air-water data of Rudzinski and co-workers [13-15]).

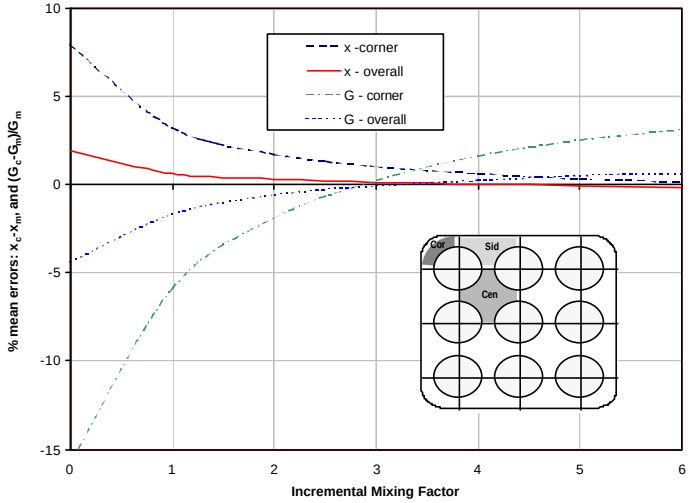

Figure 7: Variation of mean errors with incremental mixing factor (GE 3x3 rod bundle experiment).

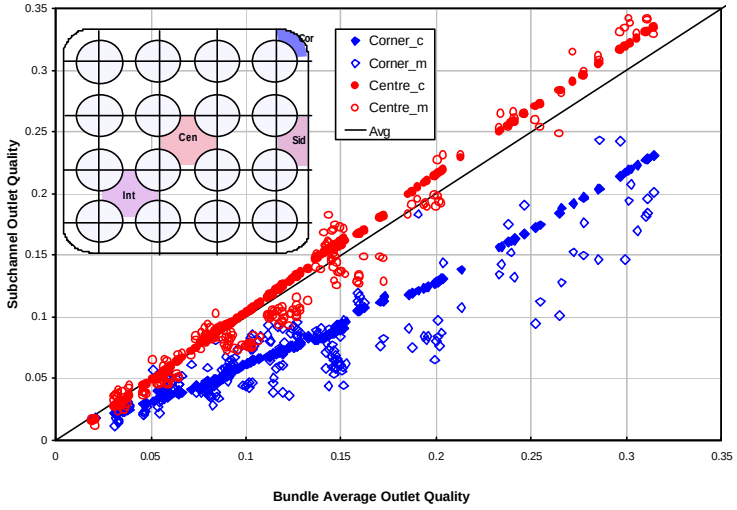

Figure 8: Comparison between predicted (c) and measured (m) qualities in outlets of corner and centre subchannels of PELCO-S experiments.

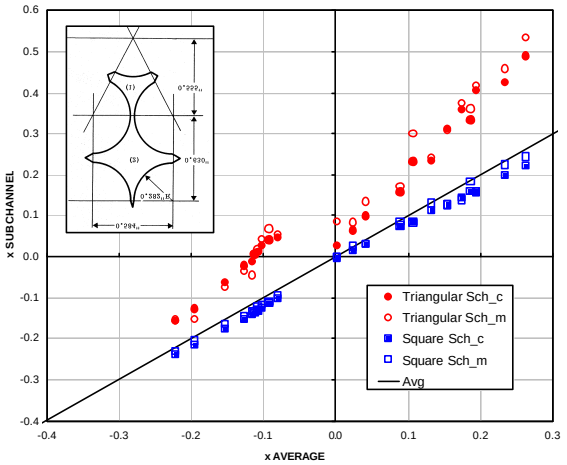

Figure 9: Comparison of predicted (c) and measured (m) subchannel outlet qualities in PNL twin-subchannel experiment (0.5 mm gap).

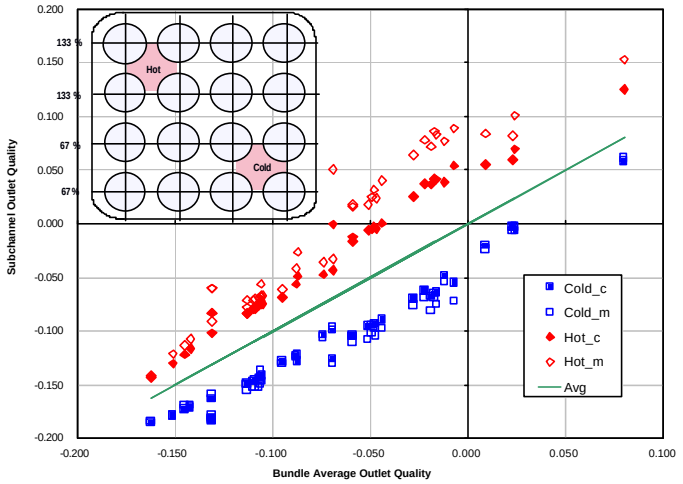

Figure 10: Comparison of predicted (c) and measured (m) qualities in outlets of "hot" and "cold" subchannels in Columbia experiments (second series).

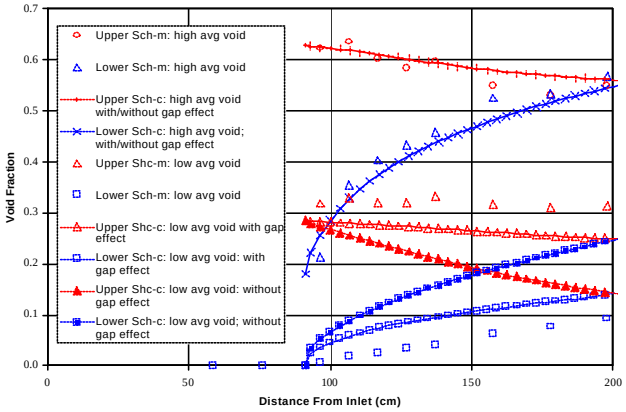

Figure 11: Comparison of predicted (c) and measured (m) axial variation of void fraction in École Polytechnique twin-subchannel experiments in horizontal air-water flow.

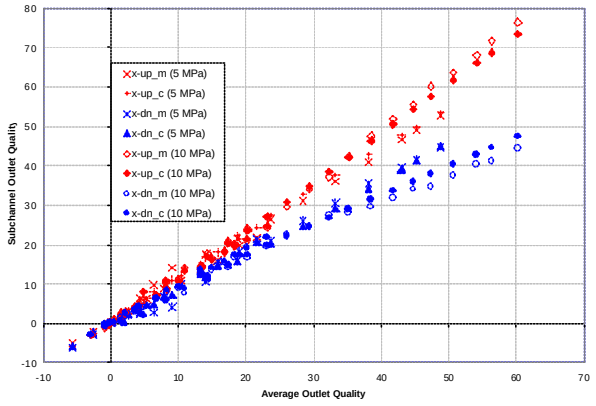

Figure 12: Comparison of predicted (c) and measured (m) subchannel outlet qualities in of AECL-CRL twin-subchannel experiments in horizontal, steam-water flow (5 and 10 MPa).